N-heterocyclic carbene complexes of silver and gold as novel tools against breast cancer progression

Carmela Saturnino[b§], Ines Barone[a§], Domenico Iacopetta[a], Annaluisa Mariconda[c], Maria Stefania Sinicropi[a*], Camillo Rosano[d*], Antonella Campana[a], Stefania Catalano[a], Pasquale Longo[c†] and Sebastiano Andò[a†].

[a]Department of Pharmacy, Health and Nutritional Sciences, University of Calabria, 87036, Arcavacata di Rende, Italy.
[b]Department of Pharmacy, University of Salerno, 84084 Fisciano, Salerno, Italy.
[c]Department of Chemistry and Biology, University of Salerno, 84084 Fisciano, Salerno, Italy.
[d]UOS Proteomics IRCCS AOU San Martino-IST National Institute for Cancer Research, Largo R. Benzi 10, Genoa, Italy.

§These authors contributed equally to the manuscript.

Running Title: *NHC complexes as anticancer agents*

*Corresponding authors:
Tel.: +39 0984 493200; fax: +39 0984 493107.
E-mail address: s.sinicropi@unical.it (M.S. Sinicropi).
Tel.: +39 010 5558337; fax: +39 010 555 8228
E-mail address: camillo.rosano@hsanmartino.it (C. Rosano).

†Joint senior authors

ABSTRACT

Background: Metal carbenic complexes have received considerable attention in both the catalysis and biological fields for their potential applications in cancer and antimicrobial therapies.

Results: A small series of new silver and gold N-heterocyclic carbene (NHC) complexes has been designed and synthesized. Amongst the tested complexes, one compound was particularly active in inhibiting anchorage-dependent and -independent breast cancer proliferation, and inducing cell apoptosis via a mitochondria-related process. The antitumor activity was associated to the transcriptional activation of the tumor suppressor gene p53 in an Sp1-dependent manner, as evidenced by biological and docking studies.

Conclusions: Our results highlight the importance and the versatility of NHC complexes of gold and silver as useful tools against breast cancer progression.

Introduction

Breast cancer represents the most frequently diagnosed cancer and the leading cause of cancer death in women worldwide, with approximately 1.7 million cases (25% of all cancers) and 521,900 deaths recorded in 2012 [1]. Based on both tumor biology and clinical factors, breast cancers are usually treated with a combination of surgery, radiotherapy, endocrine therapy (e.g. tamoxifen), biologic therapy (e.g. herceptin) and chemotherapy (e.g. platinum-based agents). Chemotherapy regimens are also currently used as treatment of choice for advanced-stage/metastatic disease, but are associated with severe adverse effects. Indeed, the most widely used platinum-based anticancer drug *cis*-platin has several limitations, such as neurotoxicity, nephrotoxicity, ototoxicity and development of intrinsic and acquired resistance in some cancer cells [2]. In addition, *cis*-platin presents a limited aqueous solubility, and is chemically incompatible with thiols. Therefore, looking for novel antitumoral metal-containing molecules with lower toxicity and higher stability is urgently needed to prolong patient survival and improve their quality of life.

Recently, several metal complexes have been investigated for their potential anticancer activities [3-9]. Among them, metal N-heterocyclic carbene (NHC) complexes are receiving growing interest in pharmaceutical research, as they readily fit the requirements for an efficient drug design, fast optimization and stability [10-12]. These complexes have the general formula L_nMX_m (Figure 1), where M is the metal that constitutes the centre of the reaction, L is the carbene, namely the ligand capable of influencing the electronic properties of the metal and, consequently, the possible catalytic activity of the complex, and X is a not carbenic ligand. In most cases, it can be a halide, a carboxylate or an alkoxide anion. A particular type of carbene is L_nM in which the metal has an oxidation state equal to zero.
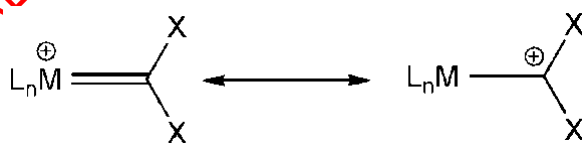

Figure 1. Carbene metal complex structures

Three types of complexes between a carbene and a transition metal have been described so far by Fischer [13], Schrock [14,15], and Arduengo-Wanzlick [16]. Chemically, they are able to form strong coordinate covalent bonds with various transition metal centres through σ-donation and ρ-back-donation, and saturation or aromaticity of the NHC ligand and the volume of attached side chains influence the stability and reactivity of the complexes [17-19]. Taking advantage of their fascinating chemical properties, different examples of NHC complexes of silver and gold have been

biologically evaluated, but also platinum or other transition metals seem to have promising properties in biomedical sciences [7,20-23]. In particular, Ag-NHCs have long been used as antimicrobial agents for their high stability [24], as they can overcome the drawbacks associated with conventional silver antibiotics including resistance and fast loss of activity [25-27]. Some of them also exhibited 'in vitro' antitumor effects [28]. However, the Ag-complexes may display less cytotoxic activity than the corresponding Au-complexes toward cancer cancer cell lines [29]. Indeed, Au–NHCs exhibit a wide range of biological activities, including antiarthritic [30] antimicrobial [31] and especially antitumor ones. Over the last ten years, there was a growing number of literature reports regarding the anticancer properties of Au (I/III)-NHC complexes in different cellular background, such as melanoma, breast, prostate and hepatocellular carcinoma cell lines. It has been proved that Au-NHC complexes can differently impact cell cycle distribution, expressions of several key regulators of apoptosis, caspase activation, mitochondrial integrity, and intracellular ROS generation [32-35]. For instance, a recent paper has shown that an Au-NHC complex was able to induce anti-melanoma effects 'in vitro' and 'in vivo' by p53 up-regulation [36].

Due to this knowledge, the main goal of the present report was to synthesize novel NHC complexes of silver and gold, whose structures were realized to evaluate the influence of increased lipophilicity on their pharmacological effects, as known from the literature [37]. Indeed, the lipophilic cation delocalized can pass through biological membranes more quickly and concentrate into organelles, mainly in the mitochondria, of cancer cells. NHC-ligands lipophilicity was increased through the functionalization of the nitrogen atoms with lipophilic substituents. Starting from the imidazole, it was evaluated the effect of different substituents on N-1 atom on the pharmacological activity. Particularly, the position 1 was substituted with a 2-cyclopentanol (L1), 2-cycloesanol (L2) and 2-hydroxy-2-phenylethyl (L3) side chains and in position 3 a methyl group was always present (Figure 2). Moreover, we prepared silver and gold NCH-complexes with the aim to evaluate the importance of the metal (*i.e* silver in **AgL1**, **AgL2**, **AgL3** and gold in **AuL1**, **AuL2** and **AuL3**). The obtained complexes have been studied for their antitumor properties in human breast cancer cells and the underlying molecular mechanism has been investigated in detail by biological assays and macromolecular docking studies, in order to shed more light on the possible ligand-protein binding modes. Specifically, we have demonstrated that one of the tested compound, **AuL3**, was particularly active in inhibiting growth and inducing apoptosis of breast cancer cells, without exerting any effects in normal breast epithelial cells. Mechanistically, this compound was able to bind the transcription factor Sp1 and to stimulate the transcription of the tumor suppressor gene p53 in an Sp1-dependent manner.

4
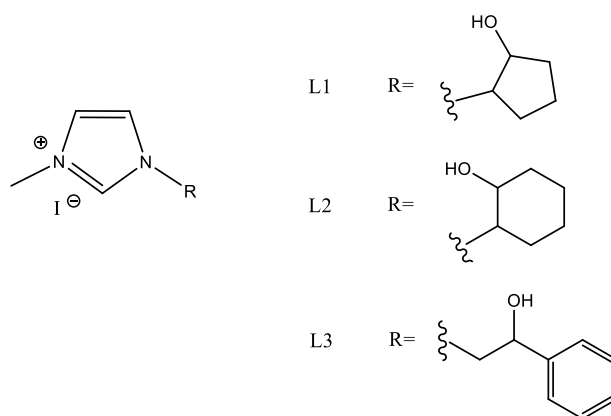
Figure 2: NHC pro-ligands **L1**, **L2** and **L3**

Materials and methods

Chemistry

All manipulations were carried out under oxygen- and moisture-free atmosphere in an MBraun MB 200 glove-box. All the solvents were thoroughly deoxygenated and dehydrated under argon by refluxing over suitable drying agents; while NMR deuterated solvents (Euriso-Top products) were kept in the dark over molecular sieves.

The organic compounds imidazole, styrene oxide, cyclohexene oxide, cyclopentene oxide and iodomethane (Strem, Aldrich) were used as received. The silver (I) oxide Ag_2O was purchased from Aldrich. ^1H NMR, homodecoupled ^1H NMR and ^{13}C NMR spectra were recorded at 298 K on a Bruker Avance 400 spectrometer operating at 400 MHz (^1H) and 100 MHz (^{13}C) and referred to internal tetramethylsilane. Fourier transform infrared (FT-IR) spectra were obtained at a resolution of 2.0 cm^{-1} with a Bruker-Vector 22 FT-IR spectrometer equipped with a deuterated triglycine sulfate (DTGS) detector and Ge/KBr beam splitter. The frequency scale was internally calibrated to 0.01 cm^{-1} using a He-Ne reference laser. Thirty-two scans were signal-averaged to reduce spectral noise. ESI-MS spectra were performed on a Quattro Micro triple quadrupole mass spectrometer equipped with an electrospray ion source. The elemental analyses for C, H, N were recorded on a Thermo-Finnigan Flash EA 1112 and were performed according to standard microanalytical procedures. The elemental analyses for I, Ag were carried out by atomic absorption spectrophotometer AAnalyst model 100 (Perkin Elmer) equipped hollow-cathode lamp Lumina Au (Perkin Elmer) using the software AAwinLabAnalyst. Gold was determined with a burner (FIAS-100) air-acetylene flame. Solution of Au at known concentration prepared from a stock solution of 1 g/l (Carlo Erba) was used as standards. The instrument was set at zero using a 1% solution of

5

HNO$_3$. Sample scripts were analyzed along with their white. Chloride was determined indirectly by reaction of AgNO$_3$ with Cl$^-$, precipitation of AgCl which was dissolved in Na$_2$S$_2$O$_3$. Silver content in the solution was determined by FAAS and the chloride content was calculated using the content of silver. The molar conductance of 10^{-3} M solutions of the gold complexes in CH$_2$Cl$_2$ solvent were measured on a Mettler Toledo Conductivity Sensor LE703 model. All the measurements were taken at room temperature for freshly prepared solutions.

Synthesis of pro-ligands and of silver(I)-NHC complexes

The synthesis of imidazolium salts (imidazolium *N*-methyl-*N'*-cyclopentan-2-ol-iodide **L1**, imidazolium-*N*-methyl-*N′*-cyclohexane-2-ol-iodide **L2,** *N*-methyl-*N'*-[(2-hydoxy-2-phenyl)ethyl] imidazolium iodide **L3**) and of the respective silver complexes (**AgL1, AgL2, AgL3**) were carried out in the same way as reported in [38].

Synthesis of gold(I)-NHC complexes

Complexes **AuL1, AuL2** and **AuL3** were synthesized by transmetallation between the appropriate Ag(I)–NHC complex (**AgL1, AgL2, AgL3**) and chloro(dimethylsulfide)gold(I) [(Me$_2$S)AuCl] according to the reported procedure in the literature [39].

General procedure. To a solution of the silver complex (**AgL1** or **AgL2** or **AgL3**) in CH$_2$Cl$_2$ a stoichiometric amount of (Me$_2$S)AuCl was added. The mixture was left to stir for 4 hours at room temperature. After this time it was filtered through celite and the solvent was removed in vacuo. The crude product was washed in hexane to obtain a yellow powder in good yield.

Complex AuL1 (bis-[N-methyl, N'(cyclopentane-2ol)-imidazole-2-ylidine]gold(I)]+[di-chloro-gold]-)

For the synthesis of *AuL1* the amount of silver complex precursor *AgL1* was 7,21•10^{-4} mol in 51,5 ml of CH$_2$Cl$_2$.

Yield: 46,7%

^{1}H NMR (400 MHz, CD$_2$Cl$_2$): 6.94 (s,1H, NC*H*CH), 7.01 (s, 1H, NCHC*H*), 4.81 (m, 1H, OC*H*), 4.47 (m, 1H, NC*H*), 3.83 (s, 3H, NC*H*$_3$), 2.56 (m, 2H, OCHC*H*$_2$), 2.24 (m, 2H, NCHC*H*$_2$), 1.75 (m, 2H, CH$_2$C*H*$_2$CH$_2$)

^{13}C NMR (100 MHz, CD$_2$Cl$_2$): 169.5 (N*C*N), 124.5 (N*C*HCH,) 122.0 (NCH*C*H), 78.4 (O*C*H), 69.5 (N*C*H), 45.6 (N*C*H$_3$), 39.9 (OCH*C*H$_2$), 34.0 (NCH*C*H$_2$), 28.2 (CH$_2$*C*H$_2$CH$_2$).

Elemental analysis: found (%):C 27.12; H 3.64; Au 49.45; Cl 8.62; N 6.96; O 3.89 Calc. for C$_9$H$_{15}$AuClN$_2$O (%): C 27.05; H 3.78; Au 49.29; Cl 8.87; N 7.01; O 4.00

Mass spectrum: 531 [Au(L1)$_2$]$^+$

Complex AuL2 (bis-[N-methyl, N'(cyclohexane-2ol)-imidazole-2-ylidine]gold(I)]+[di-chloro-gold]-)

For the synthesis of **AuL2** the amount of silver complex precursor *AgL2* was $1{,}25 \cdot 10^{-3}$ mol in 89 ml of CH_2Cl_2.

Yield: 49,9%

^{1}H NMR (400 MHz, CD_2Cl_2): 6.99 (s,1H, NC*H*CH), 7.01 (s, 1H, NCHC*H*), 5,48 (s, 1H, O*H*CH) 4.48 (m, 1H, OC*H*), 3.62 (m, 1H, NC*H*), 3.69 (s, 3H, NC*H*$_3$), 2.29 (m, 2H, OCHC*H*$_2$), 2.00 (m, 2H, NCHC*H*$_2$), 1.57 (m, 2H, OCHCH$_2$C*H*$_2$), 1.40 (m, 2H, NCHCH$_2$C*H*$_2$).

^{13}C NMR (100 MHz, $CDCl_3$): 178.9 (N*C*N), 131.5 (N*C*HCH,) 126.9 (NCH*C*H) 72.9 (O*C*H), 67.4 (N*C*H), 43.8 (N*C*H$_3$), 41.9 (OCH*C*H$_2$), 35.1 (NCHCH$_2$*C*H$_2$), 33.2 (NCH*C*H$_2$), 26.8 (OCHCH$_2$*C*H$_2$).

Elemental analysis: found (%):C 29.3; H 4.02; Au 47.81; Cl 8.49; N 6.91; O 3.72. Calc. for $C_{10}H_{17}AuClN_2O$ (%): C 29.03; H 4.14; Au 47.61; Cl 8.57; N 6.77; O 3.87.

Mass spectrum: 559 $[Au(L2)_2]^+$

Complex AuL3 bis-[N-methyl, N'(2-hydroxy-2-phenyl)ethyl)-imidazole-2-ylidine]gold(I)]+[di-chloro-gold]-)

For the synthesis of **AuL3** the amount of silver complex precursor *AgL3* was $5{,}32 \cdot 10^{-4}$ mol in 38 ml of CH_2Cl_2.

Yield: 71,8%

^{1}H NMR (400 MHz, CD_2Cl_2): δ 7.31-7.41 (m, 5H, *Ph ring*); 7.05 (d, 1H, NC*H*CHN); 6.99 (d, 1H, NCHC*H*N); 4.31 (t, 1H, C*H*OH); 3.94 (d, 2H, NC*H*$_2$); 3.71 (s, 3H, NC*H*$_3$).

^{13}C NMR (100 MHz, CD_2Cl_2): δ 185.0 (N*C*N); 141.8, 129.2, 127.5, 126.6 (*Ph ring*); 122.9 (N*C*HCHN), 122.0 (NCH*C*HN), 75.2 (O*C*H$_2$), 59.3 (N*C*H$_2$), 41.0 (N*C*H$_3$).

Elemental analysis: found (%):C 33.29; H 3.34; Au 45.42; Cl 8.01; N 6.54; O 3.53. Calc. for $C_{12}H_{15}AuClN_2O$ (%): C 33.08; H 3.47; Au 45.21; Cl 8.14; N 6.43; O 3.67.

Mass spectrum: 603 $[Au(L3)_2]^+$

Docking studies

The initial structures of **AuL3** and **AgL3** were designed and optimized in PRODRG server [40]. Docking simulations were performed using the program GOLD v.5.2.2 [41]; residues Phe 3, Ser 15, Leu 18, Ser 19, Ile 22, Lys 23 and Gln 26 were defined with flexible side chains (i.e. a free rotation of their side chains was allowed). Simulations were performed using the standard defaults: for both

7

the molecules the number of islands was set to 5, population size to 100, number of operations 100,000, the niche size of 2 and a selective pressure 1.1. ChemPLP scoring was used. Figures were drawn with the program Chimera [42,43].

Biological procedures

Plasmids

The different p53 luciferase reporter constructs, named as p53-1, -6, and -13, were provided by Dr. Safe (Texas A&M University, College Station, Texas) and were generated from the human p53 gene promoter as it follows: p53-1 (comprising the -1,800 to +12 region), p53-6 (comprising the -106 to +12 region), p53-13 (comprising the -106 to -40 region) [44].

Cell culture

Human non tumorigenic MCF-10A breast epithelial cells were cultured in Dulbecco's modified Eagle's medium-F12 supplemented with 5% Horse Serum, 0.5 µg/ml hydrocortisone, 20 ng/ml human epidermal growth factor, 100 ng/ml Cholera toxin and 10 µg/ml insulin. Human estrogen receptor (ER)-positive MCF-7 and ZR-75-1 breast cancer cells were cultured in DMEM-F12 medium containing 5% Newborn Calf Serum or 5% Fetal Bovine Serum, respectively. All media were supplemented with 2 mmol/L L-glutamine and 1 mg/ml penicillin-streptomycin. Subconfluent cell cultures, synchronized for 48 hours in DMEM-F12 without phenol red and serum (SFM), were used for all reported experiments.

Cell proliferation assays

MTT anchorage-dependent growth assays. Cell viability was determined by using the 3-(4,5-dimethylthiazol-2-yl)-2,5-diphenyltetrazolium (MTT, Sigma) assay, as previously described [45-47]. Briefly cells (2×10^4 cells/well) were plated in 24-well plates and treated as indicated. After 72 hours, 100µL of MTT stock solution in PBS (2mg/m1) was added into each well and incubated for 2 hours at 37°C followed by removal of media and solubilisation in 500µL of dimethyl sulphoxide (DMSO). Plates were shaken for 15 minutes, and the absorbance was measured at 570 nm in each well, including the blanks. At least three experiments, each one performed with 7 different doses of **AuL3, AgL3** and *cis*-platin in triplicate, were combined for IC_{50} calculations. The IC_{50} was determined using GraphPad Prism 4 Software (GraphPad Inc., San Diego, CA), as previously reported [48].

Soft agar anchorage-independent growth assays. Soft agar growth assays were performed as indicated in [49]. Briefly, cells (10^4/well) were plated in 4 ml of 0.35% agarose with 5% charcoal stripped-FBS in phenol red-free media, with a 0.7% agarose base in six-well plates. 48 hours after plating, medium containing vehicle or the different treatments was added to the top layer, and replaced every 48 hours. After 15 days, 200 µl of MTT was added to each well and incubated for 4 hours at 37°C. Plates were then placed overnight at 4°C and colonies > 50 µm diameter were counted. The data are representative of three independent experiments, each performed in triplicate.

TUNEL Assay

Cell apoptosis was investigated by TUNEL assay, following the manufacturer's instructions (CF™488A TUNEL Assay Apoptosis Detection Kit, Biotium) with small modifications. Briefly, MCF-7 cells were grown on glass coverslips, starved and then treated with AuL3 1 µM for 24 hours, washed three times with PBS, then methanol-fixed at -20°C for 15 minutes. Fixed cells were washed three times with 0.01% (V/V) Triton X-100 in PBS and incubated with 100 µL of TUNEL Equilibration Buffer for 5 minutes. After removal of Equilibration Buffer, 50 µL of TUNEL reaction mix containing 1 µL of terminal deoxynucleotidyl transferase (TdT) were added and incubated for 3 hours at 37ºC in a humid dark chamber. After the incubation, samples were washed 3 times with PBS containing 0.1% Triton X-100 and 5 mg/mL bovine serum albumin (BSA) and stained with 2-(4-amidinophenyl)-6-indolecarbamidine dihydrochloride (DAPI, Sigma) (0.2 µg/mL) for 10 minutes in a humidified dark chamber at 37ºC. After three additional washes with cold PBS, a drop of mounting solution was added. Cells were observed and imaged under an inverted fluorescence microscope (20X magnification) with excitation/emission wavelength maxima of 490 nm/515 nm (CF™488A) or 350 nm/460 nm (DAPI). Images are representative of three separate experiments.

Mitochondrial Staining

For detection of mitochondria, cells were labelled at 37°C for 20 minutes with the MitoTracker Deep Red fluorescent probe (0.01 mM, Invitrogen). After the incubation, the probe was washed out with Hank's balanced salt solution, and cell were fixed with 4% paraformaldehyde. Samples were observed and photographed with OLYMPUS-BX51 microscope equipped with a 100X oil immersion objective. Intensity of fluorescence was analyzed with Scion Image Analyzer program (Scion Corporation) and associated P values

were determined for the biological replicates by using GraphPad Prism4 Software. Images are representative of three independent experiments.

Immunoblotting analysis

Protein lysates were subjected to SDS-PAGE, as previously described [50]. After harvesting cells in cold PBS and resuspending them in lysis buffer [i) 20 mmol/L HEPES (pH 8), 0.1 mmol/L EGTA, 5 mmol/L MgCl2, 0.5 M NaC1, 20% glycerol, 1% Triton, and protease inhibitors (0.1 mmol/L sodium orthovanadate, 1% phenylmethylsulfonylfluoride, and 20 mg/ml aprotinin) for total protein extracts; ii) 250 mmol/L sucrose, 10 mmol/L HEPES (pH= 8), 10 mmol/L KCl, 1,5 mmol/L MgCl$_2$, 1 mmol/L EDTA (pH=8), 1 mmol/L EGTA (pH=8), 0,1% digitonin, 1 mmol/L phenylmethylsulfonylfluoride for cytosolic protein extracts], equal amounts of lysates were resolved on a 11-14% SDS-polyacrylamide gel, transferred to a nitrocellulose membrane, and probed with antibodies directed against p53, p21[WAF1/Cip1], PARP, cytochrome c, Bcl2, Bax, BID and GAPDH (Santa Cruz Biotechnology). The antigen-antibody complex was detected by incubation of the membranes for 1 hour at room temperature with peroxidase-coupled goat anti-mouse or anti-rabbit IgG and revealed using the enhanced chemiluminescence system (Amersham Pharmacia). The intensity of bands representing relevant proteins was measured by Scion Image laser densitometry scanning program (Scion Corporation), and standard deviations and associated P values were determined for the biological replicates by using GraphPad Prism4 Software. Immunoblots show one representative image of three separate experiments.

Real time RT-PCR Assays

Cells were grown in 10 cm dishes to 70%-80% confluence and exposed to vehicle or the different treatments as indicated. Total cellular RNA was extracted using TRIZOL reagent (Invitrogen), as suggested by the manufacturer. The purity and integrity were checked spectroscopically and by gel electrophoresis before carrying out the analytical procedures. Analysis of p53 and p21[WAF1/Cip1] gene expression was performed by real time reverse transcription-PCR in the iCycler iQ Detection System (BioRad), using SYBR Green Universal PCR Master Mix (BioRad), following the manufacturer's recommendations. Each sample was normalized on the base of its GAPDH content. Primers used for the amplification were as following: forward 5'- TCAGTCTACCTCCCGCCATA-3' and reverse 5'-TTACATCTCCCAAACATCCCT-3' (p53); forward 5'-GCATGACAGATTTCTACCACTCC -3' and reverse 5'- AAGATGTAGAGCGGGCCTTT -

3' (p21); forward 5'-CCCACTCCTCCACCTTTGAC-3' and reverse 5'-TGTTGCTGTAGCCAAATTCGTT-3' (GAPDH, house-keeping gene).

Luciferase reporter gene assay

MCF-7 cells (5×10^4 cells/well) were plated into 24-well plates with 500 µl of regular growth medium. After 24 hours, the medium was replaced with SFM, and transfection was performed by using the FuGENE 6 (Roche Diagnostic) reagent as recommended by manufacturer's protocol with the mixture containing 0.5 µg/well p53-1, p53-6 or p53-13 reporter plasmids. After 24 hours, the medium was removed and cells were treated with **AuL3** compound as indicated for 24 hours. TK Renilla luciferase plasmid (25 ng/well) was used to normalize the efficiency of the transfection. Firefly and Renilla luciferase activities of triplicate samples were measured using a Dual Luciferase kit (Promega).

Chromatin immunoprecipitation (ChIP) assays

MCF-7 cells were treated with **AuL3** compound for 3 hours, crosslinked with formaldehyde (1%) and then sonicated. Salmon sperm DNA/ protein A-agarose was used to immunoclear supernantants (1 hour, 48 °C). The precleared chromatin was immunoprecipitated with specific anti-Sp1, or anti-polymerase II antibodies (Santa Cruz Biotechnology). As a negative control, a normal mouse serum IgG was used. Pellets were washed, eluted with an elution buffer containing 1% SDS and 0.1M NaHCO$_3$, and digested with the proteinase K. DNA was obtained by phenol/chloroform/isoamyl alcohol extractions and then precipitated with ethanol. Each sample and input (5 µl) were used for real-time PCR. Real time PCR was performed in the iCycler iQ Detection System (BioRad), using SYBR Green Universal PCR Master Mix (BioRad) with the dissociation protocol used for gene amplification. The primers flanking the Spl sequence present in the p53 promoter region were the following: 5'-TTCCCCTCCCATGTGCTCAAG-3' and 5' -CCAATCCAGGGAACGTGTCA-3'. Final results were calculated using the DDC$_t$ method, using input Ct values instead of the GAPDH. As calibrator, the basal sample (vehicle-treated cells) was used.

Statistical analysis

Data were analyzed for their statistical significance using a two-tailed student's Test ($P < 0.05$, Graph Pad Prism 4). Standard deviations (S.D.) are shown.

Results and Discussion

Chemistry and Synthesis

Imidazolium-*N*-methyl-*N'*-cyclopentan-2-ol-iodide (**L1**), imidazolium-*N*-methyl-*N'*-cyclohexane-2-ol-iodide (**L2**), *N*-methyl, *N'*-[(2-hydoxy-2-phenyl)ethyl]-imidazolium iodide (**L3**) were prepared by reaction of imidazole with cyclopenteneoxide, cyclohexeneoxide and 1,2-epoxyethylbenzene, respectively, to obtain the monoalkylated product after the opening of epoxy-ring. The second reaction step, by which the second nitrogen atom is methylated using CH3I, produces the racemic mixture of the salts. In Figure 3 is reported, as an example, the reactions to obtain the pro-ligand L-3. This synthetic strategy was proposed by Arnold and co-workers, and the procedures were previously reported by some of us [51,52].
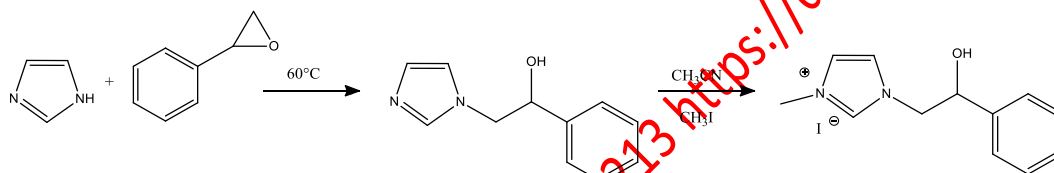
Figure 3. Synthesis of **L3** salt: *N*-methyl-*N'*-[(2-hydroxy-2-phenyl)ethyl]-imidazole iodide

Silver complexes bearing [NHC] ligands

The salts were reacted with silver oxide (Ag2O) in inert nitrogen atmosphere. In these conditions, as earlier reported, the silver oxide deprotonates the carbon 2 giving the corresponding Ag-NHC complex [38,53]. Mass spectrometry was of primary importance in determining the structure the structure of Ag-NHC compounds [54,55]. The complexes consist of [(NHC)2Ag]+ cation and of [AgI2]− anion (see Figure 4) as has been conclusively shown by the solid-state structure determined by X-ray diffraction [53].

12
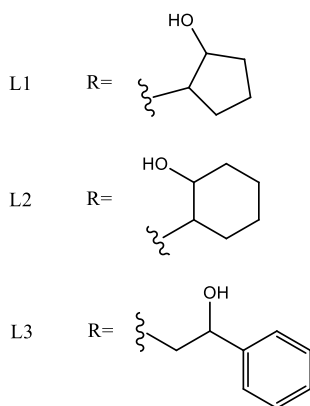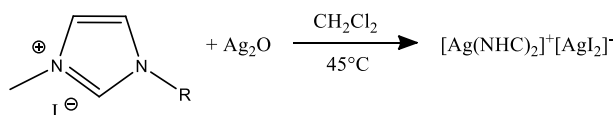
Figure 4. Synthetic scheme of Ag-NHC complexes (**AgL1**, **AgL2** and **AgL3**).

Gold complexes bearing [NHC] ligands

Complexes **AuL1**, **AuL2** and **AuL3** were synthesized by transmetallation in dichloromethane (CH_2Cl_2), between the corresponding Ag-NHC complex and the gold(I)-cloro-(dimethylsulfide) [(Me_2S)AuCl] according to the procedure reported by Baker and co-workers [39]. In Figure 5 is reported **AuL1** as example.

$$AgL1 + (Me_2S)AuCl \xrightarrow{\quad CH_2Cl_2 \quad} AuL1$$

Figure 5. Synthetic scheme of Au-NHC complex (**AuL1**).

A stoichiometric amount of (Me_2S)AuCl was added to a solution of the silver complex **AgL1** in CH_2Cl_2. Following the procedure reported in the experimental part, a yellow powder in good yield (46,7%) was obtained, whose MS spectrum showed a maximal peak at 531 m/z. FT-IR analysis revealed -OH absorbance at 3400 cm^{-1}, and ^1H and ^{13}C NMR spectra gave the expected signals (see Experimental part), with one sharp carbene resonance at 169.5 ppm. Elemental analysis of **AuL1** found for $C_9H_{15}AuClN_2O$ is in agreement with that calculated (see Experimental part). Mass spectrometry can provide fundamental data on the structure of compounds in the gas phase. In fact, the maximal peak intensity at 531 m/z is attributable to $[(L1)_2Au]^+$, on the other hand the elemental analysis gives a molar ratio among gold, ligand and chloride of 1:1:1. These data suggest that, as in

13

the case of silver compounds, [38] the gold complex may consist of $[(L1)_2Au]^+$ cation and of $[AuCl_2]^-$ anion. The proposed structure was supported by conductivity measurements, in fact the conductance values for the Au (I) compound determined in CH_2Cl_2, showed concentration-dependence in the range of 1.02 to 1.99 $\mu S\ cm^{-1}$ (see Table 1), confirming the electrolytic nature of the complex.

**Table 1**: Values of conductance of $[(L1)_2Au]^+[AuCl_2]^-$ measured in CH_2Cl_2, at 25 °C.

Concentration (mmol/l)	Conductivity ($\mu S \cdot cm^{-1}$)
3.31	1.02
4.41	1.58
5.43	1.91
6.55	1.66
8.18	1.52

The complexes **AuL2** and **AuL3** were prepared in the similar manner. In both cases in the FT-IR spectra is observed the absorbance of –OH group around 3400 cm^{-1}, ^1H and ^{13}C NMR spectra show the expected signals (see attribution in the Experimental part) with one sharp resonance for carbene of each complex at 178.9 and 185.0 ppm for **AuL2** and **AuL3**, respectively. The elemental analysis for two complexes (reported in Experimental part) gives a ratio among ligand, gold and chloride of 1:1:1. MS spectra show the peak leading, associated each one with the respective 559 and 603 m/z for the complexes **AuL2** and **AuL3**, respectively. Conductivity measurements confirmed the electrolytic nature of the complexes. So it is likely also accepted as true that the structure of these complexes is similar to that of $([Ag(L1)_2]^+[AgCl_2]^-)$ [38,53].

AuL3 compound inhibits anchorage-dependent and -independent growth in MCF-7 breast cancer cells

We have initially examined the ability of the synthesized compounds to affect breast cancer cell proliferation. Since 70 to 80% of newly diagnosed breast cancers are estrogen receptor (ER) and/or progesterone receptor (PR) -positive, we used as experimental model the well-characterized ER/PR-positive MCF-7 breast cancer cell line. The effects of increasing concentrations of the different compounds (**AuL1**, **AgL1**, **AuL2**, **AgL2**, **AuL3** and **AgL3**) on MCF-7 cell proliferation were tested by using MTT assay. We observed that **AuL1** and **AgL1**

14

as well as **AuL2** and **AgL2** treatments did not elicit any significant reduction in growth (Figure 6A and B). In contrast, **AuL3** and **AgL3** treatments for 72 hours reduced MCF-7 cell viability in a dose-dependent manner (Figure 6C), with IC_{50} values equal to 1 µM and 4 µM, respectively (Table 2). In addition, the cytotoxicity of **AuL3** was compared to the one of the commonly used anticancer drugs *cis*-platin (data not shown). The results of continuous cisplatin exposure in MTT assays showed that it was able to produce 50% growth inhibition (IC_{50}) at 80.23 ± 5.3 µM in MCF-7 cells, indicating that **AuL3** was about 80 times more cytotoxic than *cis*-platin. A second approach we have employed was to evaluate the antiproliferative effects mediated by these compounds using anchorage-independent soft agar growth assay, an assay that better reflects *in vivo* three-dimensional growth (Figure 6D). Consistently with the MTT assay data, **AuL3** and **AgL3** treatments significantly reduced colony formation in a dose-dependent manner, with the highest decrease induced by **AuL3**, whereas **AuL1**, **AgL1**, **AuL2** and **AgL2** treatments did not affect the capability of MCF-7 cells to form colonies in soft agar. Importantly, the prolonged **AuL3** and **AgL3** treatments up to 72 hours induced no antiproliferative response in non tumorigenic MCF-10A breast epithelial cells (Figure 6E). Taken together, these results demonstrated that **AuL3** was the most active molecule in inducing growth inhibition in MCF-7 breast cancer cells, probably because of its lipophilic features and golden presence, compared to the other synthetized compounds.

15
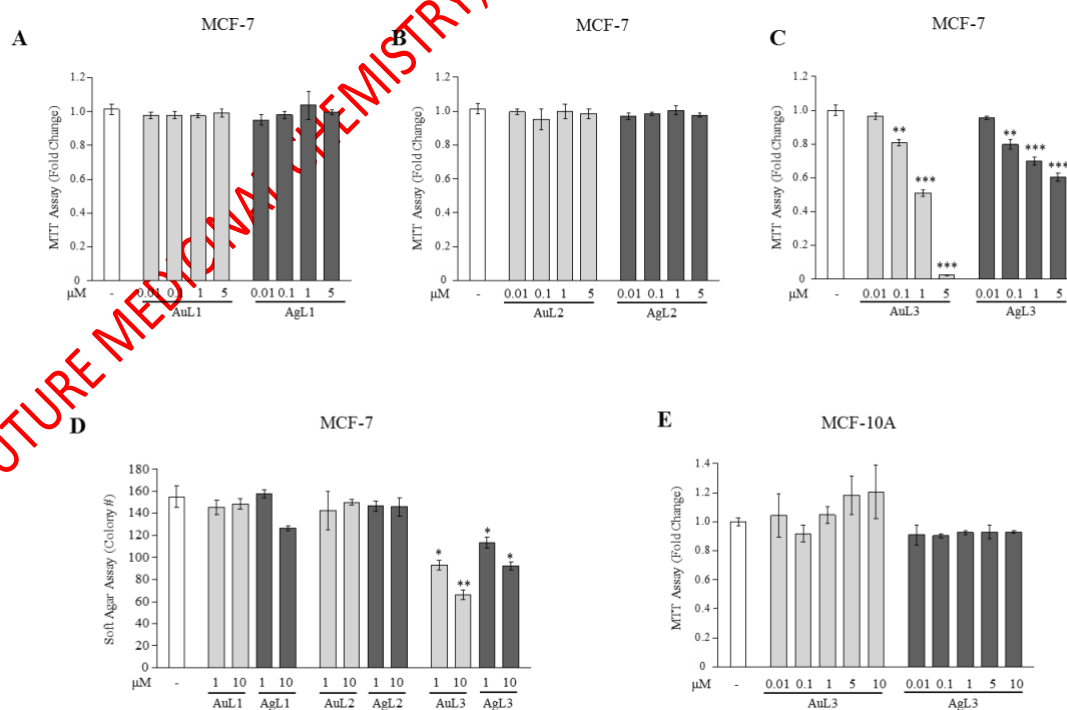
**Figure 6. Effects of Au-NHC and Ag-NHC complexes on MCF-7 breast cancer cell growth.**

MTT assays in MCF-7 breast cancer cells treated with vehicle (-), or **AuL1/AgL1 (A), AuL2/AgL2 (B), AuL3/AgL3 (C)** at 0.01, 0.1, 1, and 5 µM of concentrations for 72 hours. Cell proliferation is expressed as fold change compared to control (vehicle-treated cells). The values represent the means ± S.D. of three different experiments, each performed with triplicate samples. **(D)** MCF-7 cells were plated in soft agar and then treated with vehicle (-) or the different compounds as indicated. Cells were allowed to grow for 14 days and the number of colonies >50 µm were quantified and the results were graphed. Data are the mean colony number ± S.D. of three plates and representative of three independent experiments. **(E)** MTT assays in MCF-10A non tumorigenic breast epithelial cells treated with vehicle (-), or increasing concentrations of **AuL3** or **AgL3** (0.01, 0.1, 1, 5 and 10 µM) for 72 hours. Cell proliferation is expressed as fold change compared to control (vehicle-treated cells). The values represent the means ± S.D. of three different experiments, each performed with triplicate samples. *, P <0.05; **, P < 0.005; ***, P < 0.0005.

AuL3 compound induces apoptosis in MCF-7 breast cancer cells

In order to determine the role of apoptosis in cell growth inhibition induced by **AuL3** treatment, we used two different approaches. First, we evaluated the proteolysis of poly (ADP-ribose) polymerase (PARP), a well-recognized cellular substrate of mammalian caspases, by immunoblotting analysis (Figure 7A). We found an increase in the levels of the proteolytic form of PARP (86 kDa) in MCF-7 breast cancer cells after **AuL3** treatment, as compared to the control. Secondly, the TUNEL assay was performed to assess DNA fragmentation as a key event in the process of apoptosis. As shown in Figure 7B, a high percentage of TUNEL-positive cells was observed in MCF-7 cells treated with **AuL3** at 1 µM of concentration. Mitochondria play a crucial role in the regulation of apoptosis and many chemotherapeutic agents that induce cell apoptosis trigger mitochondrial dysfunction when added to intact cells [56,57]. Interestingly, several gold-carbene complexes have been examined as anticancer agents with antimithocondrial activity [58]. Thus, we investigated whether the observed apoptotic effects induced by **AuL3** exposure in MCF-7 cells were due to impaired mitochondria. Mitochondria were labelled with a mitochondrial-targeted probe, MitoTracker Deep Red FM, and mitochondrial staining was monitored. In non-apoptotic (vehicle-treated) cells, intact mitochondria exhibited a clear perinuclear red fluorescence; whereas in cells treated with **AuL3**, the fluorescence intensity of the probe decreased in a time-dependent manner, implying a reduction of mitochondrial content. Figure 7C shows the changes of MCF-7 cell fluorescence as a result of drug treatment. Consistently with the release of cytochrome c into the extramitochondrial milieu under apoptotic conditions [59], a significant increase of cytochrome c levels in the cytosolic fractions of MCF-7 cells after 24 and 48h of treatment with **AuL3** was detected (Figure 7D). The maintenance of mitochondrial integrity is highly dependent on the Bcl-2 family of proteins [60,61]. The expression levels of the anti-apoptotic protein Bcl-2 were

16

slightly decreased in **AuL3**-treated MCF-7 cells, whereas exposure of MCF-7 cells to AuL3 resulted in an increased expression of the pro-apoptotic proteins Bax and BID (Figures 7D). These results highlight the potential of **AuL3** compound to target the mitochondrial cell death pathway.
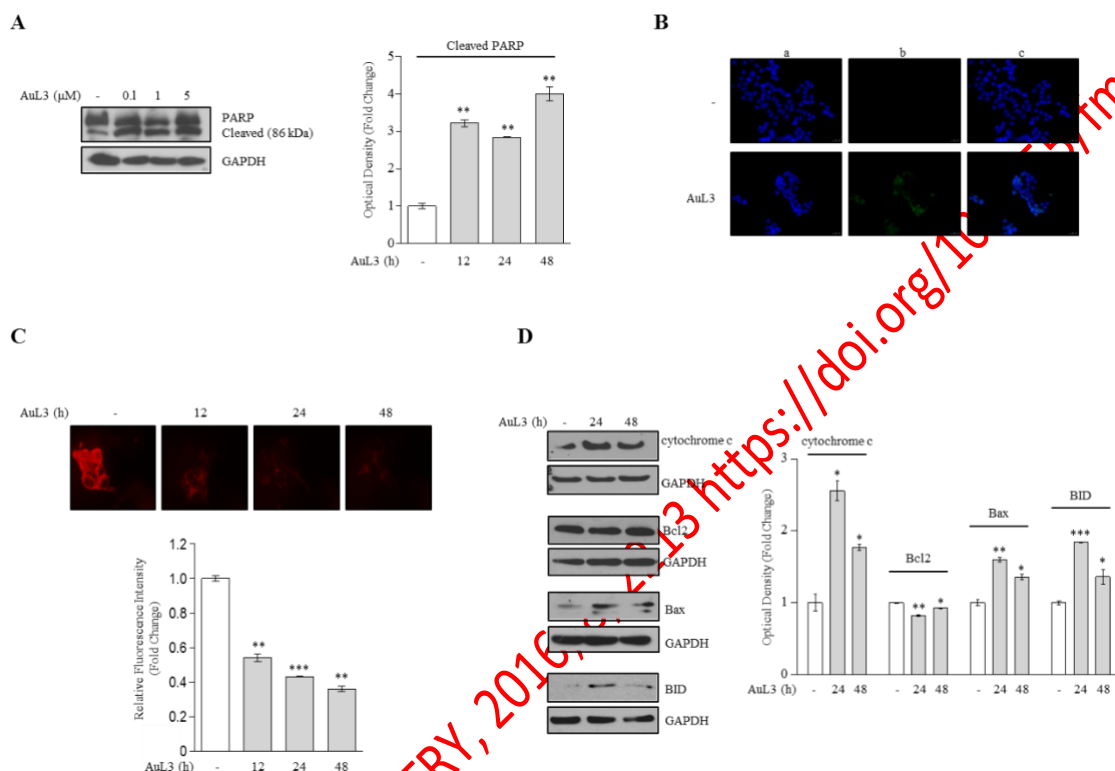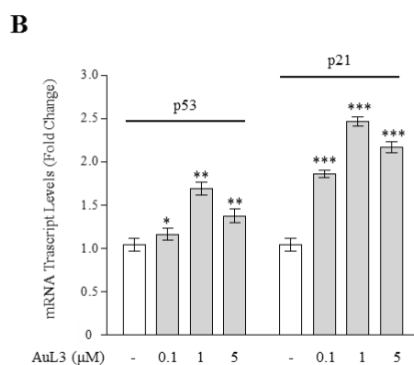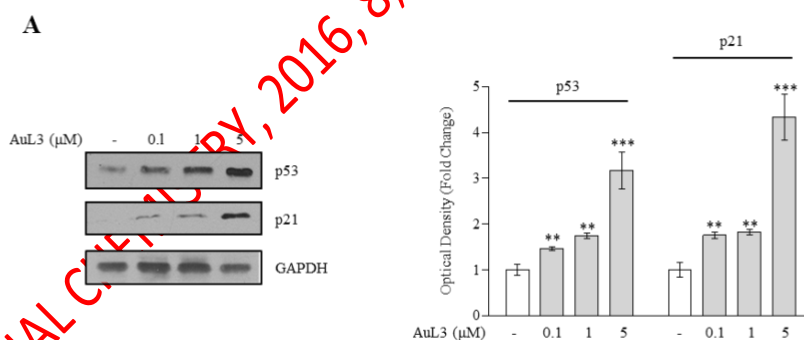

Figure 7. Apoptotic effects of AuL3 compound in MCF-7 breast cancer cells.

(A) *Left panel*, immunoblot of PARP protein from extracts of MCF-7 cells treated with vehicle (-) or **AuL3** at 0.1, 1 and 5 µM of concentrations for 24 hours. GAPDH was used as control for equal loading and transfer. *Right panel*, the histograms represent the means ± S.D. of three separate experiments in which band intensities were evaluated in terms of optical density arbitrary units and expressed as fold change compared to vehicle-treated samples and normalized for GAPDH content. **(B)** MCF-7 cells were treated with vehicle (-) or **AuL3** at a concentration of 1 µM for 24 hours. After treatment, cells were cold-methanol fixed and subjected to TUNEL assay. After DAPI incubation to stain nuclei, fixed cell were observed and imaged under an inverted fluorescence microscope (20X magnification): a) TUNEL staining, b) DAPI, c) overlay. Images are representative of three separate experiments. **(C)** Mitochondria staining with MitoTracker Deep Red Fluorescent probe in cells treated with vehicle (-) or **AuL3** at 1 µM for 12, 24 and 48 hours. Fluorescence images are shown (*upper panel*) and fluorescence levels are quantitated (*lower panel*) from three separate experiments. **(D)** *Left panel*, immunoblot of cytochrome c, Bcl2, Bax and BID from extracts of MCF-7 cells treated with vehicle (-) or **AuL3** at 1 µM for 24 and 48 hours. GAPDH was used as control for equal loading and transfer. *Right panel*, the histograms represent the means ± S.D. of three separate experiments in which band intensities were evaluated in terms of optical density arbitrary units and expressed as fold change compared to vehicle-treated samples and normalized for GAPDH content. *, $P < 0.05$; **, $P < 0.005$; ***, $P < 0.0005$.

17

__AuL3__ treatment increases p53 and p21$^{WAF1/Cip1}$ expression in MCF-7 breast cancer cells

Since the tumor suppressor gene p53 is required for checkpoint control during cell cycle progression in response to different factors and participates in the apoptotic cascade even by directly acting on multiple mitochondrial targets [62,63], we examined the potential ability of **AuL3** to modulate the expression of p53 along with its natural target gene p21$^{WAF1/Cip1}$. Cells were treated with **AuL3** at 0.1, 1 and 5µM concentrations and whole cell lysates were then analysed using immunoblotting analysis. As shown in Figure 8A, **AuL3** treatment significantly increased p53 and p21$^{WAF1/Cip1}$ protein expression. Accordingly, real time RT-PCR revealed an induction of both p53 and p21$^{WAF1/Cip1}$ mRNA levels in MCF-7 cells after 24 hour treatment with all the different doses of **AuL3** (Figure 8B). These results prompted us to investigate whether the up-regulatory effects of **AuL3** compound on p53 expression may be due to its ability to influence p53 gene transcriptional activity.

Figure 8. Up-regulation of p53 and p21 expression by AuL3 compound in MCF-7 breast cancer cells. (A) *Left panel,* immunoblots of p53, and p21$^{WAF1/Cip1}$ from extracts of MCF-7 cells treated with vehicle (-) or **AuL3** at 0.1, 1 and 5 µM of concentrations for 48 hours. GAPDH was used as a control for equal loading and transfer. *Right panel,* the histograms represent the mean ± S.D. of three separate experiments in which band intensities were evaluated in terms of optical density arbitrary units and expressed as fold change compared to vehicle-treated samples and normalized for GAPDH content. (B) p53 and p21 $^{WAF1/Cip1}$ mRNA expression, evaluated by real time RT-PCR, in MCF-7 cells treated with vehicle (-) or **AuL3** (0.1, 1, 5 µM) for 24 hours. Each sample was normalized to its GAPDH mRNA content. *, $P < 0.05$; **, $P < 0.005$: ***, $P < 0.0005$.

To evaluate whether **AuL3** may transactivate the p53 promoter gene, MCF-7 cells were transiently transfected with a luciferase reporter construct (named as p53-1) containing the upstream region of the p53 gene spanning from -1,800 to +12 bp (Figure 9A) and treated with increasing concentrations of **AuL3** for 24 hours. We observed a significant activation of p53-1 after treatment with **AuL3** compound (Figure 9B). To identify the region within the p53 promoter responsible for **AuL3**-mediated transactivation, we performed functional assays using p53-deleted constructs containing putative binding motifs for CTF-1/YY1, nuclear factor-Y (NF-Y), nuclear factor-κB (NFκB) and Sp1-like proteins (GC) (schematically shown in Figure 9A). The responsiveness to **AuL3** compound was still maintained in cells transfected with the p53-6 plasmid encoding the region from -106 to +12, whereas it was no longer observed in the presence of the p53-13 construct encoding the sequence from -106 to -40 (Figure 9C). Therefore, the region from -40 to +12, which contains the GC-rich/Sp1 motifs, was required for mediating the stimulatory effects of **AuL3** on p53 promoter gene expression. To confirm the specific involvement of Sp1 region in AuL3-mediated p53 transactivation, ChIP assays were performed. Using specific antibodies against Sp1, and RNA-polymerase II, protein-chromatin complexes were immunoprecipitated from cells treated with or without **AuL3** compound for 3 hours. The resulting precipitated DNA was then quantified using real time PCR with primers spanning the Sp1-binding element within the p53 promoter region. As shown in Figure 9D, Sp1 recruitment was significantly increased upon **AuL3** treatment. These results were well correlated with an enhanced association of RNA-polymerase II to the p53 regulatory region (Figure 9E). Our findings demonstrated that the ability of **AuL3** compound to stimulate p53 transcription is dependent on the transcription factor Sp1.

19
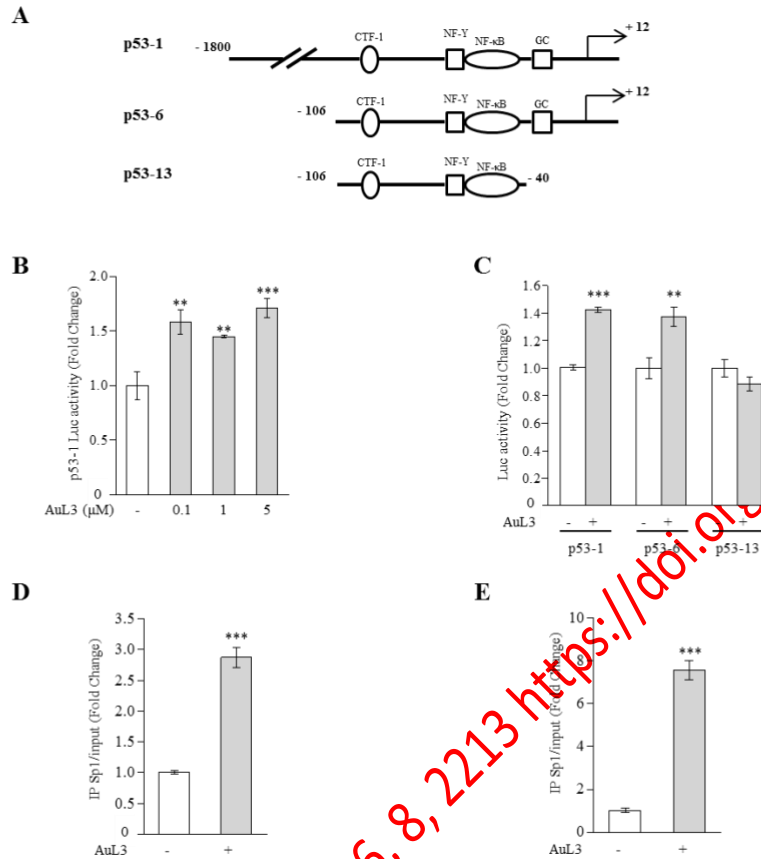
Figure 9. Effects of AuL3 compound on p53 gene promoter luciferase reporter constructs.
(**A**) Schematic map of the p53 promoter fragments used in this study. CTF-1, CCAAT-binding transcription factor-1; NF-Y, nuclear factor-Y; NFκB, nuclear factor-κB, GC, GC- rich motif. (**B**) MCF-7 cells were transiently transfected with p53 gene promoter luciferase reporter construct p53-1 and treated for 24 hours with vehicle (-) or **AuL3** at 0.1, 1, and 5 µM of concentrations. (**C**) MCF-7 cells were transiently transfected with p53 gene promoter luciferase reporter constructs (p53-1, p53-6, p53-13) and treated for 24 hours with vehicle (-) or **AuL3** (1 µM). The luciferase activities were normalized to the *Renilla* luciferase as internal transfection control and data were reported as fold change. MCF-7 cells were treated with vehicle (-) or **AuL3** (1 µM, 3 hours), then crosslinked with formaldehyde, and lysed. The precleared chromatin was immunoprecipitated with anti-Sp1 (**D**), and anti-RNA polymerase II (**E**) antibodies. A 5µl volume of each sample and input was analyzed by real time PCR using specific primers to amplify p53 promoter sequence, including the GC-rich motif. Columns are the means ± S.D. of three independent experiments, each performed in triplicate. **, $P < 0.005$; ***, $P < 0.0005$.

Sp1 is a well-investigated factor that has been shown to be involved through the transcriptional regulation of many genes in several cellular processes, including cell differentiation, growth, and apoptosis [64]. Because of the Sp1-dependent up-regulatory effects on p53 gene transcription mediated by **AuL3** compound, we evaluated the potential binding mode of **AuL3** to Spl by molecular docking studies using as molecular target, the

Zinc finger domain of Sp1 (PDB code 1SP1) [65]. We also evaluated docking interaction of **AgL3** with Sp-1. The binding site center was positioned as the OG atom of Ser 19 and the volume encompassed by 20Å from that atom was considered as the binding cleft. **AuL3** and **AgL3** have a similar binding mode to Sp1 (Figure 10, panels A and B). The top ranked poses show a fitness ranking of 61.34 and 57.93, respectively. Both the **AuL3** and **AgL3** moieties form hydrogen bond with Ser 19 residue and halogen bond with Lys 23 residue, hydrophobic interactions with Ile 22 and a π- π stacking with Phe 3 (Figure 10, panel A and B). A small displacement of the silver atom with respect to the gold atom was the only significant difference between the two poses (Figure 10, panel C), this would affect the lesser antitumor activity of **AgL3** respect to **AuL3.**
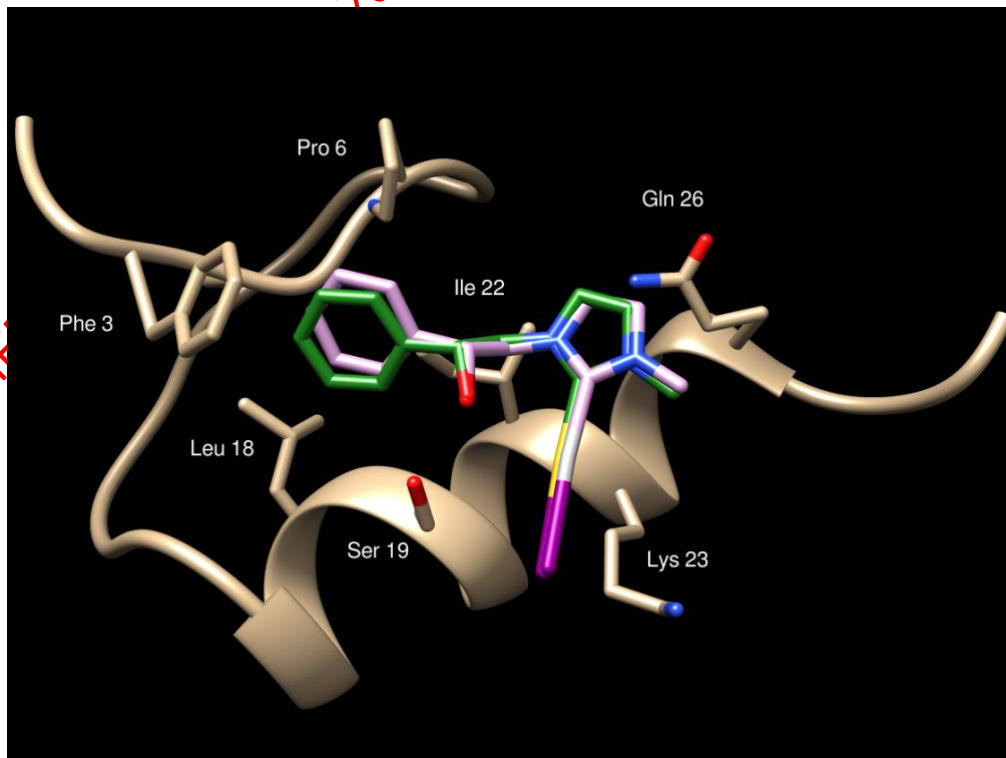
A
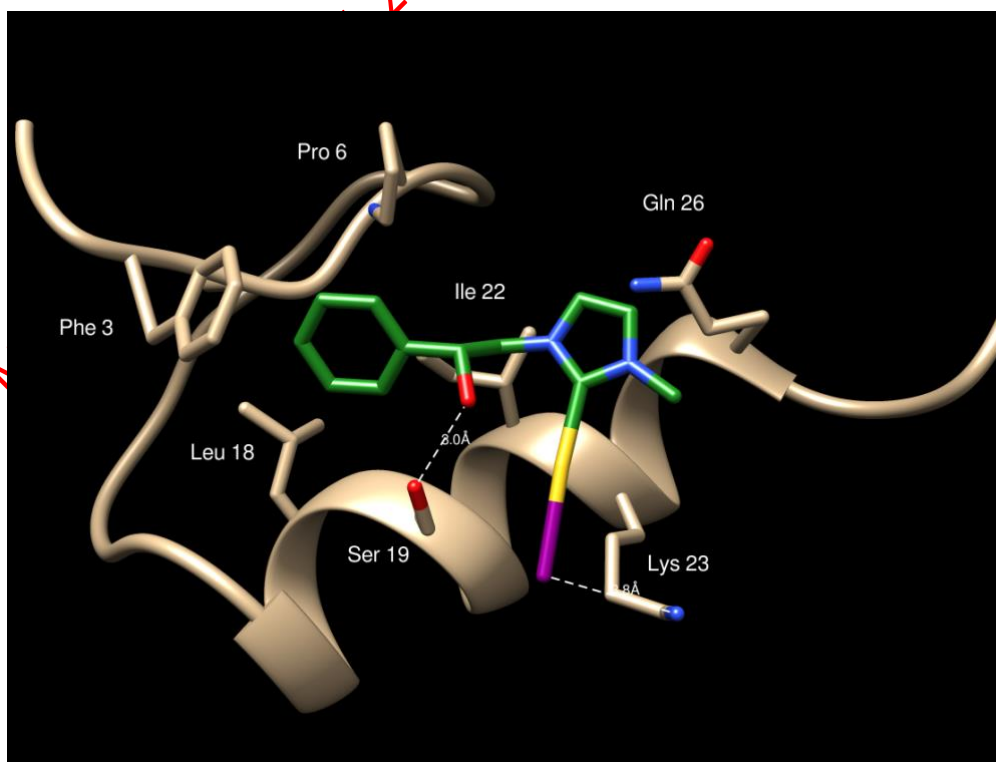
B
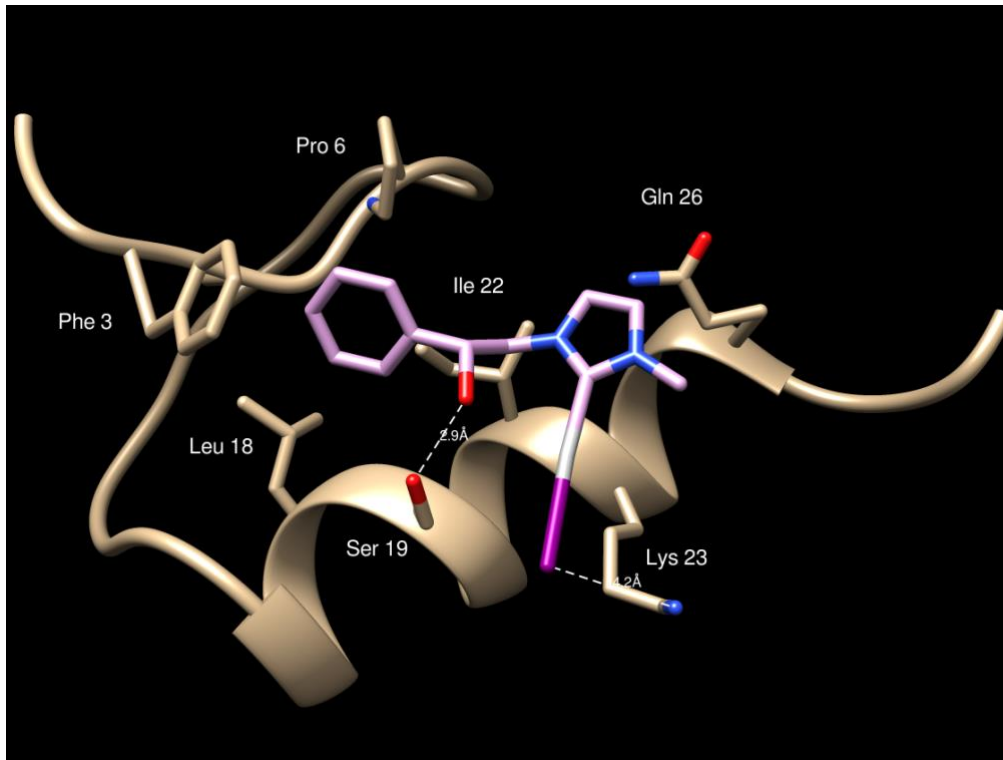
C

Figure 10: **Binding mode of AuL3 and AgL3 to Sp1 zinc finger domain.**
The three dimensional structure of the Zinc finger domain from Transcription Factor Sp1 is reported as a brown ribbon. Residues involved in ligands binding are evidenced as sticks. Panels A and B report the poses of **AuL3** and **AgL3**, respectively. The two binding modes are superposed in Panel C.

*Effects of **AuL3** in ZR-75-1 breast cancer cells*

To extend the results obtained, we tested the effects of **AuL3** compound in affecting growth of another human ERα-positive breast cancer cell line, named as ZR-75-1 cells. By using MTT assay, we demonstrated that **AuL3** compound for 72 hours inhibited cell survival in a dose-dependent fashion with IC_{50} values equal to 2.6 µM (Figure 11A, and Table 2). In addition, as previously shown for MCF-7 cells, we found augmented PARP cleaved levels as well as increased expression of both p53 and p21[WAF1/Cip1] proteins in ZR-75-1 cells after treatment with increasing concentrations of **AuL3** (Figure 11B). These data confirmed that **AuL3** compound inhibits cell growth and induces apoptosis in different breast cancer cell background through p53 up-regulation.
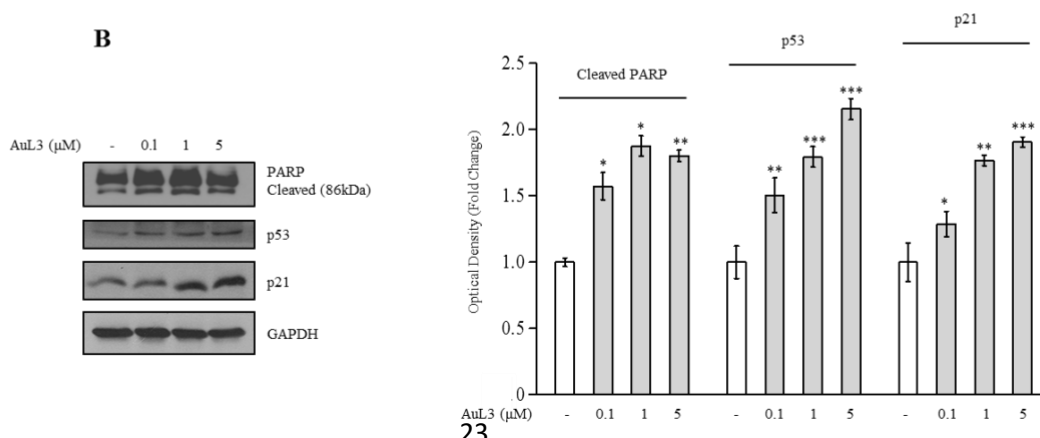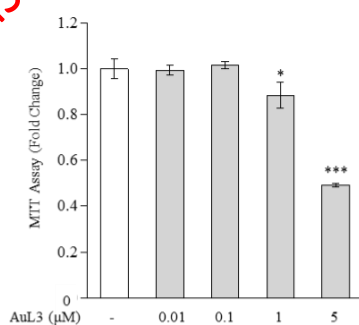
Figure 11. Effects of AuL3 treatment on ZR-75-1 breast cancer cell growth.
(A) MTT assays in ZR-75-1 breast cancer cells treated with vehicle (-), or increasing concentrations of AuL3 (0.01, 0.1, 1, and 5 µM) for 72 hours. Cell proliferation is expressed as fold change compared to control (vehicle-treated cells). The values represent the means ± S.D. of three different experiments, each performed with triplicate samples. **(B)** *Left panel,* immunoblots showing PARP, p53, and p21$^{WAF1/CiP1}$ protein expression from extracts of ZR-75-1 cells treated with vehicle (-) or **AuL3** at 0.1, 1 and 5µM of concentrations for 48 hours. GAPDH was used as a control for equal loading and transfer. *Right panel,* the histograms represent the mean ± S.D. of three separate experiments in which band intensities were evaluated in terms of optical density arbitrary units and expressed as fold change compared to vehicle-treated samples and normalized for GAPDH content. *, $P < 0.05$; **, $P < 0.005$; ***, $P < 0.0005$.

Conclusions

Herein, we have reported the synthesis and the biological evaluation of three silver NHC and of three new gold NHC complexes as valid therapeutic tools against breast cancer progression. These metallopharmaceuticals were projected introducing lipophilic substituents on the carbene structure in order to increase the ability to cross the biological membranes. As demonstrated, the most active antitumor compounds were **AgL3** and **AuL3**, holding a lipophilic structure, and they did not affect the proliferation of non-tumorigenic epithelial breast cells. Particularly, **AuL3** exhibited lower IC$_{50}$ values (1 and 2.6 µM, on MCF-7 and ZR-75-1 breast cancer cells, respectively) respect to **AgL3**, suggesting the importance of gold for the higher antitumor activity. Moreover, we have demonstrated that the antitumor activity of **AuL3** is due to the up-regulation of p53 and p21$^{WAF1/Cip1}$ expression, dependent on the transcription factor Spl. The role of Sp1 has been further confirmed by molecular docking studies. These outcomes are interesting in the metallopharmaceutics research and open up a wide range of possibilities to obtain versatile carbene complexes, with a variety of ligands that may provide a novel arsenal of useful anticancer tools as a valid alternative to the most used *cis*-platin.

Future perspective

These outcomes may be enlarged in order to ameliorate the antitumor activity and diminish the toxicity of metal-complexes based-drugs. In this way, new classes of anticancer compounds able to act on specific targets will be developed and used as valid therapeutic strategies to the most traditional chemotherapeutic agents.

Executive summary

Three silver and three new gold N-heterocyclic carbene (NHC) complexes were reported

The three new gold NHC complexes were synthesized by transmetallation reaction

AuL3 inhibits breast cancer growth and triggers apoptosis

Mechanistically, **AuL3** induces Sp1-mediated p53 up-regulation

Key terms

Transmetallation:

A type of chemistry reaction by which ligands are transferred from one metal to another.

Docking simulation:

Computational simulation technique used to predict the binding orientation of a candidate ligand into the active site of protein targets.

TUNEL assay:

An apoptosis detection system based on the measurement of nuclear DNA fragmentation, an important biochemical hallmark of apoptosis.

Luciferase reporter gene assay:

Powerful and sensitive tool for cell biology research useful for assaying gene expression and quantifying any changes in transcription.

References

Paper of special note have been highlighted as:

*of interest; **of considerable interest

1. Ferlay J, Soerjomataram I, Dikshit R *et al.* Cancer incidence and mortality worldwide: sources, methods and major patterns in GLOBOCAN 2012. *Int. J. Cancer.* 136(5), E359-386 (2015).
2. Berners-Price SJ. Activating platinum anticancer complexes with visible light. *Angew. Chem. Int. Edit.* 50(4), 804-805 (2011).
3. Sirignano E, Saturnino C, Botta A *et al.* Synthesis, characterization and cytotoxic activity on breast cancer cells of new half-titanocene derivatives. *Bioorg. Med. Chem. Lett.* 23(11), 3458-3462 (2013).
4. Napoli M, Saturnino C, Sirignano E, Popolo A, Pinto A, Longo P. Synthesis, characterization and cytotoxicity studies of methoxy alkyl substituted metallocenes. *Eur. J. Med. Chem.* 46(1), 122-128 (2011).
5. Saturnino C, Napoli M, Paolucci G *et al.* Synthesis and cytotoxic activities of group 3 metal complexes having monoanionic tridentate ligands. *Eur. J. Med. Chem.* 45(9), 4169-4174 (2010).
6. Grisi F, Costabile C, Grimaldi A, Viscardi C, Saturnino C, Longo P. Synthesis of Unsaturated Macrocycles by Ru-Catalyzed Ring-Closing Metathesis: A Comparative Study. *Eur. J. Org. Chem.* 30, 5928-5934 (2012).
7. Saturnino C, Sirignano E, Botta A *et al.* New titanocene derivatives with high antiproliferative activity against breast cancer cells. *Bioorg. Med. Chem. Lett.* 24(1), 136-140 (2014).
8. Chimento A, Saturnino C, Iacopetta D *et al.* Inhibition of human topoisomerase I and II and anti-proliferative effects on MCF-7 cells by new titanocene complexes. *Bioorg. Med. Chem.* 23(22), 7302-7312 (2015).
9. Sirignano E, Pisano A, Caruso A *et al.* Different 6-Aryl-Fulvenes Exert Anti-proliferative effects on Cancer Cells. *Anti-cancer Agents Me.* 15(4), 468-474 (2015).
10. Hu CQ, Li X, Wang W, Zhang RY, Deng LB. Metal-N-Heterocyclic Carbene Complexes as Anti-Tumor Agents. *Current Med. Chem.* 21(10), 1220-1230 (2014).
11. Gautier A, Cisnetti F. Advances in metal-carbene complexes as potent anti-cancer agents. *Metallomics.* 4(1), 23-32 (2012).
12. Perfetto A, Costabile C, Longo P, Bertolasi V, Grisi F. Probing the relevance of NHC ligand conformations in the Ru-catalysed ring-closing metathesis reaction. *Chem.-Eur J.* 19(32), 10492-10496 (2013). ***(Reports the preparation of suitable substituted NHC backbone)**
13. Fischer EO. On the Way of Carbene and Carbyne Complexes. *Adv. Organomet. Chem.* 14, 1-32 (1976).
14. Guggenberger LJ, Schrock RR. Structure of bis(cyclopentadienyl)methylmethylenetantalum and the estimated barrier to rotation about the tantalum-methylene bond. *J. Am. Chem. Soc.* 97 (22), 6578–6579 (1975).
15. Schrock RR, Fellmann JD. Multiple metal-carbon bonds. 8. Preparation, characterization, and mechanism of formation of the tantalum and niobium neopentylidene complexes, M(CH2CMe3)3(CHCMe3). *J. Am. Chem. Soc.* 100 (11), 3359–3370 (1978).
16. Arduengo AJ, Ill, Harlow RL, Kline M. A stable crystalline carbene. *J. Am. Chem. Soc.*, 113, 361-363 (1991).
17. Cavallo L, Correa A, Costabile C, Jacobsen H. Steric and electronic effects in the bonding of N-heterocyclic ligands to transition metals. *J. Organomet. Chem.* 690(24-25), 5407-5413 (2005).
18. Hu XL, Castro-Rodriguez I, Olsen K, Meyer K. Group 11 metal complexes of N-heterocyclic carbene ligands: Nature of the metal-carbene bond. *Organometallics.* 23(4), 755-764 (2004).
19. Nemcsok D, Wichmann K, Frenking G. The significance of pi interactions in group 11 complexes with N-heterocyclic carbenes. *Organometallics.* 23(15), 3640-3646 (2004).
20. Oehninger L, Rubbiani R, Ott I. N-Heterocyclic carbene metal complexes in medicinal chemistry. *Dalton T.* 42(10), 3269-3284 (2013).
21. Patil SA, Patil SA, Patil R *et al.* N-heterocyclic carbene metal complexes as bio-organometallic antimicrobial and anticancer drugs. *Future Med. Chem.* 7(10), 1305-1333 (2015). ****(Focuses on the**

current development and advances in the preparation/characterization of NHC-metal complexes and their biomedical potential)

22. Sirignano E, Saturnino C, Botta A *et al.* Synthesis, characterization and cytotoxic activity on breast cancer cells of new half-titanocene derivatives. *Bioorg. Med. Chem. Lett.* 23(11), 3458-3462 (2013).

23. Bruno G, Nicolo F, Loschiavo S, Sinicropi MS, Tresoldi G. Synthesis and Spectroscopic Properties of Di-2-Pyridyl Sulfide (Dps) Compounds - Crystal-Structure of [Ru(Dps)2cl2]. *J. Chem. Soc. Dalton Trans.* 1, 17-24 (1995).

24. Klasen HJ. A historical review of the use of silver in the treatment of burns. II. Renewed interest for silver. *Burns.* 26(2), 131-138 (2000).

25. Melaiye A, Simons RS, Milsted A *et al.* Formation of water-soluble pincer silver(I)-carbene complexes: A novel antimicrobial agent. *J. Med. Chem.* 47(4), 973-977 (2004).

26. Hindi KM, Siciliano TJ, Durmus S *et al.* Synthesis, stability, and antimicrobial studies of electronically tuned silver acetate N-heterocyclic carbenes. *J. Med. Chem.* 51(6), 1577-1583 (2008).

27. Youngs WJ, Knapp AR, Wagers PO, Tessier CA. Nanoparticle encapsulated silver carbene complexes and their antimicrobial and anticancer properties: A perspective. *Dalton T.* 41(2), 327-336 (2012).

28. Medvetz DA, Hindi KM, Panzner MJ, Ditto AJ, Yun YH, Youngs WJ. Anticancer Activity of Ag(I) N-Heterocyclic Carbene Complexes Derived from 4,5-Dichloro-1H-Imidazole. *Metal-based Drugs*, 2008, 384010 (2008).

29. Li Y, Liu GF, Tan CP, Ji LN, Mao ZW. Antitumor properties and mechanisms of mitochondria-targeted Ag(I) and Au(I) complexes containing N-heterocyclic carbenes derived from cyclophanes. *Metallomics.* 6(8), 1460-1468 (2014).

30. Talib J, Beck JL, Ralph SF. A mass spectrometric investigation of the binding of gold antiarthritic agents and the metabolite [Au(CN)2]- to human serum albumin. *J. Biol. Inorg. Chem.* 11(5), 559-570 (2006).

31. Ozdemir I, Denizci A, Ozturk HT, Cetinkaya B. Synthetic and antimicrobial studies on new gold(I) complexes of imidazolidin-2-ylidenes. *Appl. Organomet. Chem.* 18(7), 318-322 (2004).

32. Yan JJ, Chow ALF, Leung CH, Sun RWY, Ma DL, Che CM. Cyclometalated gold(III) complexes with N-heterocyclic carbene ligands as topoisomerase I poisons. *Chem. Commun.* 46(22), 3893-3895 (2010).

33. Wang CH, Shih WC, Chang HC *et al.* Preparation and Characterization of Amino-Linked Heterocyclic Carbene Palladium, Gold, and Silver Complexes and Their Use as Anticancer Agents That Act by Triggering Apoptotic Cell Death. *J. Med. Chem.* 54(14), 5245-5249 (2011).

34. Das Adhikary S, Bose D, Mitra P, Das Saha K, Bertolasi V, Dinda J. Au(I)- and Pt(II)-N-heterocyclic carbene complexes with picoline functionalized benzimidazolin-2-ylidene ligands; synthesis, structures, electrochemistry and cytotoxicity studies. *New J. Chem.* 36(3), 759-767 (2012).

35. Mui YF, Fernandez-Gallardo J, Elie BT *et al.* Titanocene-Gold Complexes Containing N-Heterocyclic Carbene Ligands Inhibit Growth of Prostate, Renal, and Colon Cancers in Vitro. *Organometallics.* 35(9), 1218-1227 (2016).

36. Nandy A, Dey SK, Das S, Munda RN, Dinda J, Das Saha K. Gold (I) N-heterocyclic carbene complex inhibits mouse melanoma growth by p53 upregulation. *Mol. Cancer.* 13 (2014). ***(Shows the 'in vitro' and 'in vivo' anti-melanoma properties of a newly synthesized Au-NHC complex)**

37. Hahn FE, Jahnke MC. Heterocyclic carbenes: Synthesis and coordination chemistry. *Angew. Chem. Int. Edit.* 47(17), 3122-3172 (2008).

38. Napoli M, Saturnino C, Cianciulli EI *et al.* Silver(I) N-heterocyclic carbene complexes: Synthesis, characterization and antibacterial activity. *J. Organomet. Chem.* 725, 46-53 (2013). ***(Reports the synthesis of new silver-complexes with stability to hydrolysis and antibacterial activity)**

39. Baker MV, Barnard PJ, Berners-Price SJ *et al.* Synthesis and structural characterisation of linear Au(I) N-heterocyclic carbene complexes: New analogues of the Au(I) phosphine drug Auranofin. *J. Organomet. Chem.* 690(24-25), 5625-5635 (2005).

40. Schuttelkopf AW, van Aalten DM. PRODRG: a tool for high-throughput crystallography of protein-ligand complexes. *Acta Crystallogr. D. Biol. Crystallogr.* 60(Pt 8), 1355-1363 (2004).

41. Sinicropi MS, Lappano R, Caruso A *et al.* (6-bromo-1,4-dimethyl-9H-carbazol-3-yl-methylene)-hydrazine (carbhydraz) acts as a GPER agonist in breast cancer cells. *Curr. Top. Med. Chem.* 15(11), 1035-1042 (2015).

42. Pettersen EF, Goddard TD, Huang CC *et al.* UCSF Chimera--a visualization system for exploratory research and analysis. *J. Comput. Chem.* 25(13), 1605-1612 (2004).

43. Iacopetta D, Madeo M, Tasco G *et al.* A novel subfamily of mitochondrial dicarboxylate carriers from Drosophila melanogaster: biochemical and computational studies. *Biochim. Biophys. Acta.* 1807(3), 251-261 (2011).

44. Qin CH, Nguyen T, Stewart J, Samudio I, Burghardt R, Safe S. Estrogen up-regulation of p53 gene expression in MCF-7 breast cancer cells is mediated, by calmodulin kinase IV-dependent activation of a nuclear factor kappa B/CCAAT-binding transcription factor-1 complex. *Mol. Endocrinol.* 16(8), 1793-1809 (2002).

45. Sala M, Chimento A, Saturnino C *et al.* Synthesis and cytotoxic activity evaluation of 2,3-thiazolidin-4-one derivatives on human breast cancer cell lines. *Bioorg. Med. Chem. Lett.* 23(17), 4990-4995 (2013).

46. Sinicropi MS, Caruso A, Conforti F *et al.* Synthesis, inhibition of NO production and antiproliferative activities of some indole derivatives. *J. Enz. Inhib. Med. Ch.* 24(5), 1148-1153 (2009).

47. Caruso A, Chimento A, El-Kashef H *et al.* Antiproliferative activity of some 1,4-dimethylcarbazoles on cells that express estrogen receptors: part I. *J. Enz. Inhib. Med. Ch.* 27(4), 609-613 (2012).

48. Grande F, Barone I, Aiello F *et al.* Identification of novel 2-(1H-indol-1-yl)-benzohydrazides CXCR4 ligands impairing breast cancer growth and motility. *Fut. Med. Chem.* 8(2), 93-106 (2016). ***(Highlights the identification and synthesis of leads useful for a rational design of broad-spectrum therapeutics active in breast cancer)**

49. Rechoum Y, Rovito D, Iacopetta D *et al.* AR collaborates with ERalpha in aromatase inhibitor-resistant breast cancer. *Breast Cancer Res. Tr.* 147(3), 473-485 (2014).

50. Gu GW, Barone I, Gelsomino L *et al.* Oldenlandia diffusa extracts exert antiproliferative and apoptotic effects on human breast cancer cells through ER alpha/Sp1-mediated p53 activation. *J. Cell. Physiol.* 227(10), 3363-3372 (2012).

51. Arnold PL, Rodden M, Davis KM, Scarisbrick AC, Blake AJ, Wilson C. Asymmetric lithium(I) and copper(II) alkoxy-N-heterocyclic carbene complexes; crystallographic characterisation and Lewis acid catalysis. *Chem. Commun.* (14), 1612-1613 (2004).

52. Bocchino C, Napoli M, Costabile C, Longo P. Synthesis of Octahedral Zirconium Complex Bearing [NHC-O] Ligands, and Its Behavior as Catalyst in the Polymerization of Olefins. *J. Polym. Sci. Pol. Chem*. 49(4), 862-870 (2011).

53. Mariconda A, Grisi F, Costabile C, Falcone S, Bertolasi V, Longo P. Synthesis, characterization and catalytic behaviour of a palladium complex bearing a hydroxy-functionalized N-heterocyclic carbene ligand. *New J. Chem.* 38(2), 762-769 (2014). ****(Shows the synthetic route to obtain complexes possessing functionalized, unsymmetrical substituted NHC ligand and transmetallation reaction)**

54. Kascatan-Nebioglu A, Panzner MJ, Tessier CA, Cannon CL, Youngs WJ. N-Heterocyclic carbene-silver complexes: A new class of antibiotics. *Coordin. Chem. Rev.* 251(5-6), 884-895 (2007).

55. Wang HMJ, Lin IJB. Facile synthesis of silver(I)-carbene complexes. Useful carbene transfer agents. *Organometallics.* 17(5), 972-975 (1998).

56. Makin G, Dive C. Recent advances in understanding apoptosis: new therapeutic opportunities in cancer chemotherapy. *Trends Mol. Med.* 9(6), 251-255 (2003).

57. Debatin KM, Poncet D, Kroemer G. Chemotherapy: targeting the mitochondrial cell death pathway. *Oncogene.* 21(57), 8786-8803 (2002).

58. Barnard PJ, Baker MV, Berners-Price SJ, Day DA. Mitochondrial permeability transition induced by dinuclear gold(I)-carbene complexes: potential new antimitochondrial antitumour agents. *J. Inorg. Biochem.* 98(10), 1642-1647 (2004).

59. Gogvadze V, Orrenius S, Zhivotovsky B. Multiple pathways of cytochrome c release from mitochondria in apoptosis. *BBA-Bioenergetics*, 1757(5-6), 639-647 (2006).

60. Brenner D, Mak TW. Mitochondrial cell death effectors. *Curr Opin Cell Biol*, 21(6), 871-877 (2009).

61. Czabotar PE, Lessene G, Strasser A, Adams JM. Control of apoptosis by the BCL-2 protein family: implications for physiology and therapy. *Nat. Rev. Mol. Cell. Bio.* 15(1), 49-63 (2014).

62. Mihara M, Erster S, Zaika A *et al.* p53 has a direct apoptogenic role at the mitochondria. *Mol. Cell.* 11(3), 577-590 (2003).

63. Murphy ME, Leu JIJ, George DL. p53 moves to mitochondria - A turn on the path to apoptosis. *Cell Cycle* 3(7), 836-839 (2004).
64. Suske G. The Sp-family of transcription factors. *Gene.* 238(2), 291-300 (1999).
65. Narayan VA, Kriwacki RW, Caradonna JP. Structures of zinc finger domains from transcription factor Sp1 - Insights into sequence-specific protein-DNA recognition. *J. Biol. Chem.* 272(12), 7801-7809 (1997).

Table 2. IC$_{50}$ of **AuL3** and **AgL3** compounds for MCF-7 and ZR-75-1 breast cancer cells on anchorage-dependent growth.

Cell Lines	IC$_{50}$ (µmol/L) AuL3	95% confidence interval	IC$_{50}$ (µmol/L) AgL3	95% confidence interval
MCF-7	1	0.8-1.2	4	2.1-5.8
ZR-75-1	2.6	2.2-3.2		